A stress recovery signaling network for enhanced flooding tolerance in *Arabidopsis thaliana*

Elaine Yeung[a], Hans van Veen[a], Divya Vashisht[a], Ana Luiza Sobral Paiva[b], Maureen Hummel[c], Tom Rankenberg[a], Bianka Steffens[d], Anja Steffen-Heins[e], Margret Sauter[f], Michel de Vries[g], Robert C. Schuurink[g], Jérémie Bazin[h], Julia Bailey-Serres[a,c,1], Laurentius A. C. J. Voesenek[a], and Rashmi Sasidharan[a,1]

[a]Plant Ecophysiology, Institute of Environmental Biology, Utrecht University, 3584 CH Utrecht, The Netherlands; [b]Programa de Pós-Graduação em Genética e Biologia Molecular, Departamento de Genética, Universidade Federal do Rio Grande do Sul, Porto Alegre, 91509-900 Brazil; [c]Department of Botany and Plant Sciences, Center for Plant Cell Biology, University of California, Riverside, CA 92521; [d]Plant Physiology, Philipps University, 35032 Marburg, Germany; [e]Institute of Human Nutrition and Food Science, Kiel University, 24118 Kiel, Germany; [f]Plant Developmental Biology and Plant Physiology, Kiel University, 24118 Kiel, Germany; [g]Plant Physiology, Swammerdam Institute for Life Sciences, University of Amsterdam, 1098 XH Amsterdam, The Netherlands; and [h]IPS2, Institute of Plant Science-Paris Saclay (CNRS, Institut National de la Recherche Agronomique), University of Paris-Saclay, 91405 Orsay, France

Contributed by Julia Bailey-Serres, May 21, 2018 (sent for review March 5, 2018; reviewed by Mikio Nakazono and Su-May Yu)

Abiotic stresses in plants are often transient, and the recovery phase following stress removal is critical. Flooding, a major abiotic stress that negatively impacts plant biodiversity and agriculture, is a sequential stress where tolerance is strongly dependent on viability underwater and during the postflooding period. Here we show that in *Arabidopsis thaliana* accessions (Bay-0 and Lp2-6), different rates of submergence recovery correlate with submergence tolerance and fecundity. A genome-wide assessment of ribosome-associated transcripts in Bay-0 and Lp2-6 revealed a signaling network regulating recovery processes. Differential recovery between the accessions was related to the activity of three genes: *RESPIRATORY BURST OXIDASE HOMOLOG D*, *SENESCENCE-ASSOCIATED GENE113*, and *ORESARA1*, which function in a regulatory network involving a reactive oxygen species (ROS) burst upon desubmergence and the hormones abscisic acid and ethylene. This regulatory module controls ROS homeostasis, stomatal aperture, and chlorophyll degradation during submergence recovery. This work uncovers a signaling network that regulates recovery processes following flooding to hasten the return to prestress homeostasis.

flooding | ribosome footprinting | reactive oxygen species | dehydration | recovery

Plants continuously adjust their metabolism to modulate growth and development within a highly dynamic and often inhospitable environment. Climate change has exacerbated the severity and unpredictability of environmental conditions that are suboptimal for plant growth and survival, including extremes in the availability of water and temperature. Under these conditions, plant resilience to environmental extremes is determined by acclimation not only to the stress itself but also to recovery following stress removal. This is especially apparent in plants recovering from flooding. Flooding is an abiotic stress that has seen a recent global surge with dramatic consequences for crop yields and plant biodiversity (1–3). Most terrestrial plants, including nearly all major crops, are sensitive to partial to complete submergence of aboveground organs. Inundations that include aerial organs severely reduce gas diffusion rates, and the ensuing impedance to gas exchange compromises both photosynthesis and respiration. Additionally, muddy floodwaters can almost completely block light access, thus further hindering photosynthesis. Ultimately, plants suffer from a carbon and energy crisis and are severely developmentally delayed (4, 5). As floodwaters recede, plant tissues adjusted to the reduced light and oxygen in murky waters are suddenly reexposed to aerial conditions. The shift to an intensely illuminated and reoxygenated environment poses additional stresses for the plant, namely oxidative stress and, paradoxically, dehydration due to malfunctioning roots, frequently resulting in desiccation of the plant (6). Flooding can thus be viewed as a sequential stress where both the flooding and postflooding periods pose distinct stressors, and tolerance is determined by the ability to acclimate to both phases.

While plant flooding responses have been extensively studied, less is known about the processes governing the rate of recovery, particularly the stressors, signals, and downstream reactions generated during the postflood period. When water levels recede, it has been hypothesized that the combination of reillumination and reoxygenation triggers a burst of reactive oxygen species (ROS) production. Reoxygenation has been shown to induce oxidative stress in numerous monocot and dicot species (7–11) and related ROS production dependent on the abundance of ROS scavenging enzymes and antioxidant capacity of tissues (12–16). However, in the link between ROS and survival during recovery, several aspects remain vague, including the source of the ROS and whether it also has a signaling role. Mechanisms regulating shoot dehydration upon recovery also remain to be elucidated. In rice (*Oryza sativa*), the flooding tolerance-associated *SUB1A* gene also confers drought and oxidative stress tolerance during reoxygenation through increased ROS scavenging and enhanced abscisic acid (ABA) responsiveness (9). In *Arabidopsis*, ABA, ethylene, and jasmonic acid have been implicated in various aspects of postanoxic recovery (8, 16, 17). While these studies have furthered understanding of flooding recovery, the key recovery

Significance

Flooding due to extreme weather events can be highly detrimental to plant development and yield. Speedy recovery following stress removal is an important determinant of tolerance, yet mechanisms regulating this remain largely uncharacterized. We identified a regulatory network in *Arabidopsis thaliana* that controls water loss and senescence to influence recovery from prolonged submergence. Targeted control of the molecular mechanisms facilitating stress recovery identified here could potentially improve performance of crops in flood-prone areas.

Author contributions: E.Y., B.S., M.S., J.B.-S., L.A.C.J.V., and R.S. designed research; E.Y., D.V., A.L.S.P., M.H., T.R., A.S.-H., M.d.V., and J.B. performed research; E.Y., H.v.V., D.V., A.L.S.P., M.H., A.S.-H., M.d.V., R.C.S., J.B., and R.S. analyzed data; and E.Y., J.B.-S., L.A.C.J.V., and R.S. wrote the paper.

Reviewers: M.N., Nagoya University; and S.-M.Y., Academia Sinica.

The authors declare no conflict of interest.

Data deposition: The data reported in this paper have been deposited in the Sequence Read Archive (SRA) database, https://www.ncbi.nlm.nih.gov/sra (SRA accession no. SRP133870).

[1]To whom correspondence may be addressed. Email: serres@ucr.edu or r.sasidharan@uu.nl.

This article contains supporting information online at www.pnas.org/lookup/suppl/doi:10.1073/pnas.1803841115/-/DCSupplemental.

Published online June 11, 2018.

PLANT BIOLOGY

signals, hierarchical relationships between them, and molecular processes regulating variation and success of recovery remain unclear.

To identify causal mechanisms of the variation in recovery tolerance and unravel the underlying signaling network, we used two *Arabidopsis* accessions, Bay-0 and Lp2-6, differing in post-submergence tolerance. The accessions' sensitivity to complete submergence was primarily due to differences in the shoot tissue during recovery. Through genome-scale sequencing of ribosome-associated transcripts during prolonged submergence and subsequent recovery, we identified three key genes that could explain the superior recovery capacity in Lp2-6: *SENESCENCE-ASSOCIATED GENE113* (*SAG113*), *ORESARA1* (*ORE1*/*NAC6*), and *RESPIRATORY BURST OXIDASE HOMOLOG D* (*RBOHD*). In a network involving a ROS burst, ethylene, and ABA, these players regulate ROS homeostasis, stomatal aperture, and senescence to ultimately influence recovery.

Results

Submergence Recovery in Two *Arabidopsis* Accessions. *Arabidopsis* accessions Bay-0 and Lp2-6 were previously identified as sensitive and tolerant, respectively, to complete submergence based on assessment of survival at the end of a recovery period following desubmergence (18). However, further evaluation indicated that this difference in tolerance was mainly due to differences in the recovery phase (Fig. 1*A* and Movie S1). When completely submerged at the 10-leaf stage for 5 d in the dark, plants of both accessions had similar chlorophyll content (Fig. 1*B*) and shoot dry weight (*SI Appendix*, Fig. S1*A*). Following return to control growth conditions, however, the tolerant accession Lp2-6 maintained more chlorophyll (Fig. 1*B*) and increased shoot biomass (*SI Appendix*, Fig. S1*A*). Faster development of new leaves in Lp2-6 (*SI Appendix*, Fig. S1*B*) led to higher fitness based on a significantly higher seed yield (Fig. 1*C*). When Bay-0 and Lp2-6 plants were placed in darkness only, rather than submergence together with darkness, both accessions displayed some leaf senescence but no clear phenotypic differences (*SI Appendix*, Fig. S1*C*), indicating that reaeration determines the distinction in accession survival.

The different recovery survival of the accessions was attributed to the shoot, since grafting an Lp2-6 shoot to a Bay-0 root or an Lp2-6 root did not affect the high tolerance of Lp2-6 shoots. Similarly, Bay-0 shoots grafted to either Lp2-6 or Bay-0 roots had low tolerance (Fig. 1*D* and *SI Appendix*, Fig. S1*D*). Thus, only shoot traits were further investigated. In both accessions, older leaves showed the most severe submergence damage, with visible dehydration during recovery. Young leaves and the shoot meristem survived in both accessions, but intermediary leaves (leaf 5 to 7 of a 10-leaf-stage rosette, where leaf 1 is the first true leaf after cotyledon development) showed the strongest visible differences between accessions. This correlated with higher chlorophyll content in Lp2-6 intermediary leaves following desubmergence (Fig. 1*E*). Interestingly, photosynthetic capacity after desubmergence, as reflected in F_v/F_m (variable fluorescence/maximal fluorescence), was higher in Bay-0 leaves compared with Lp2-6 leaves (Fig. 1*F*). In subsequent recovery time points, however, Bay-0 intermediary leaves failed to recover toward control F_v/F_m values, whereas Lp2-6 leaves showed full recovery by 3 d following desubmergence. Lower F_v/F_m values in Bay-0 during recovery indicated more photosystem II damage, which may have prevented replenishment of starch reserves (Fig. 1*G*). Based on this characterization of Bay-0 and Lp2-6, further analyses were restricted to the intermediary leaves showing the clearest variable effects of desubmergence stress between both accessions.

Ribosome Sequencing Reveals Conserved and Accession-Specific Changes in Ribosome-Associated Transcripts During Submergence and Recovery. To identify molecular processes contributing to the observed differences in Bay-0 and Lp2-6 during submergence and recovery, the intermediary leaves showing a strong physiological response to desubmergence were subjected to an unbiased ribosome-sequencing (Ribo-seq) approach (19, 20) (Fig. 2 and *SI Appendix*, Fig. S2*A*). Translatome analysis by Ribo-seq was selected over transcriptome analysis by RNA-seq to increase the likelihood of identifying differentially regulated transcripts that were actively translated, as selective mRNA translation contributes to gene regulation in response to dynamics in oxygen, light, ROS, and ethylene (21–25). Intermediary leaves were harvested from plants at the start of the treatment (0-h control), submerged in the dark for 5 d (sub), and recovered for 3 h after desubmergence (rec) (Fig. 2*A*). Each translatome library consisted of at least 38 million reads mapped to the Col-0 genome (*SI Appendix*, Fig. S2*B*). Multidimensional scaling showed that biological replicates clustered together (*SI Appendix*, Fig. S2*C*). Furthermore, treatments and accessions clearly clustered separately. Under control conditions, the Bay-0 and Lp2-6 translatomes grouped together. As expected, the reads mapped primarily to protein-coding regions (*SI Appendix*, Fig. S2*D*).

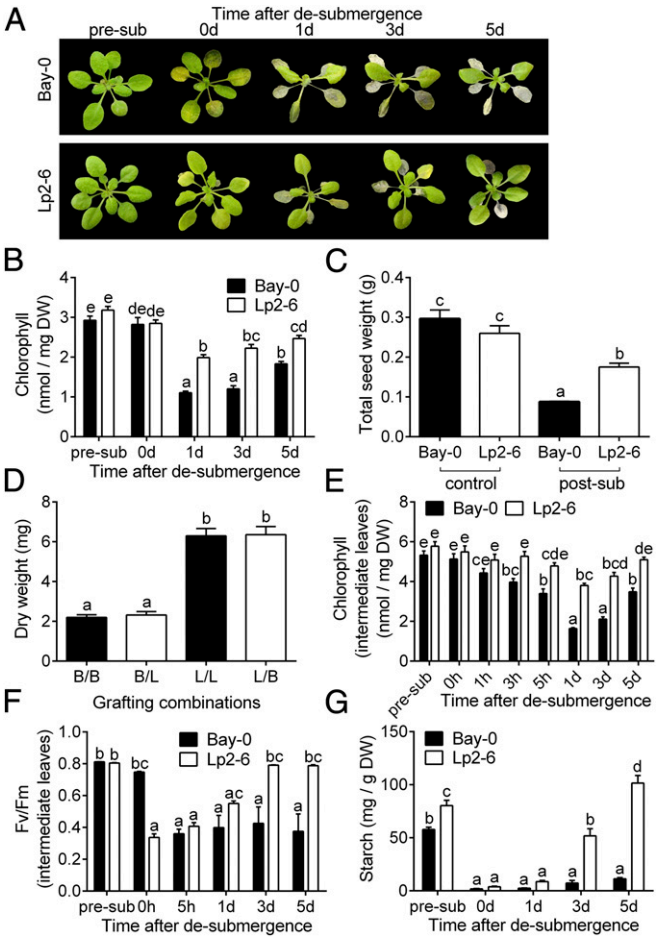

Fig. 1. Effects of complete submergence on subsequent recovery in two *Arabidopsis* accessions, Bay-0 and Lp2-6. (*A*) Representative shoots of Bay-0 and Lp2-6 before submergence (pre-sub), after 5 d of dark submergence (0 d), and 1, 3, and 5 d of recovery. (*B*) Chlorophyll content of whole rosettes (n = 9 or 10). DW, dry weight. (*C*) Total seed output of individual control and submergence recovery plants (n = 10 to 15). (*D*) Shoot dry weight of grafted plants submerged for 5 d and recovered for another 5 d under control conditions. Grafting combinations represent the accession of the shoot/root (B, Bay-0; L, Lp2-6) (n = 45 to 60). (*E*) Chlorophyll content in intermediary leaves (n = 15). (*F*) Maximum quantum efficiency of photosystem II (F_v/F_m) in intermediary leaves (n = 10). (*G*) Starch content in whole rosettes (n = 3). Data represent mean ± SEM from independent experiments. Significant difference is denoted by different letters (P < 0.05, one- or two-way ANOVA with Tukey's multiple comparisons test).

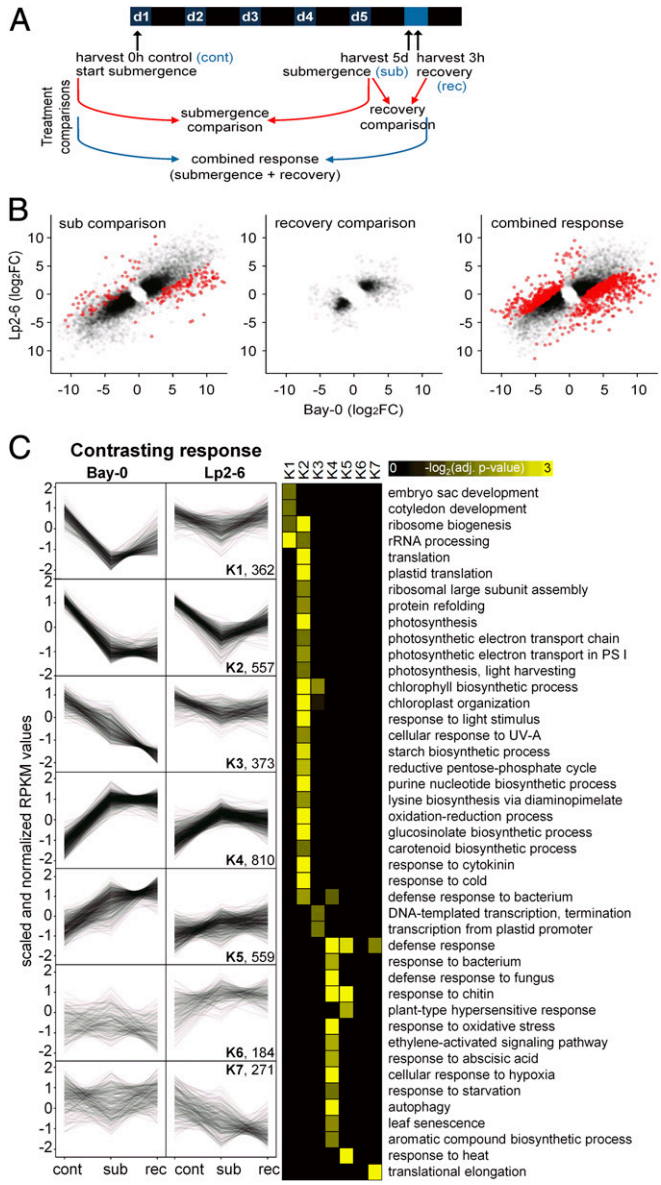

Fig. 2. Submergence and recovery induce distinct changes in ribosome-associated transcripts. (*A*) Overview of Ribo-seq experimental design and treatment comparisons. Bay-0 and Lp2-6 intermediary leaves were harvested before treatment (control, cont), 5-d dark submergence (submergence, sub), and 3 h after desubmergence (recovery, rec). The submergence effect was investigated by comparing 5-d submergence-treated samples with the 0-h control ("submergence comparison"). Both samples were harvested at the same time during the photoperiod. The recovery effect was a comparison of 5-d submerged samples with those recovered for 3 h in control air and light conditions after desubmergence ("recovery comparison"). The combined effect of submergence and recovery was determined by comparing desubmerged 3-h recovery plants with 0-h control plants ("combined response"). (*B*) Scatterplots comparing Bay-0 and Lp2-6 $\log_2$FC (fold change) under submergence comparison, recovery comparison, and combined response. Red dots represent accession × treatment DEGs ($P_{adj} < 0.05$) and black dots are remaining DEGs. (*C*) Fuzzy *K*-means clustering of genes showing different behavior in Bay-0 and Lp2-6. Control (0 h, cont), submergence (5 d, sub), and recovery (3 h, rec) conditions were individually plotted as black lines using scaled and normalized reads per kilobase per million mapped reads (RPKM) values, and the total number of DEGs in each cluster is noted. GO enrichment for each cluster is visualized as a heatmap.

A large number of genes responded significantly to the treatments, and their responses were statistically indistinguishable between the accessions (Fig. 2*B*). These similarly behaving genes were resolved into five clusters using fuzzy *K*-means clustering (*SI Appendix*, Fig. S3), and enriched gene ontology (GO) categories for these clusters were identified. In both accessions, the common response genes involved in light perception and photosynthesis were down-regulated by submergence in darkness but were not reactivated upon recovery (K1). Genes associated with the cytoplasmic translational process were also down-regulated (K2), but were up-regulated upon recovery. Other translation-associated genes were up-regulated during both submergence and recovery (K3). In contrast, responses involved in carbon limitation were strongly induced by submergence and down-regulated during recovery (K4). Stress-related GO categories involved in water deprivation and ROS increased upon submergence and rose further during recovery (K5).

To obtain an understanding of processes important for strong performance during recovery, we identified genes at each harvest time point differing in mRNA abundance between the two accessions (*SI Appendix*, Fig. S2*E*) and genes that responded to the treatments differently (*SI Appendix*, Fig. S2 *E* and *F*). Treatment-independent differences increased after submergence and increased even further after the brief recovery period. This was reflected in the number of differentially expressed genes (DEGs) in the accession-specific treatment responses, which was largest when considering the combination of submergence and recovery (Fig. 2*B* and *SI Appendix*, Fig. S2*F*).

Genes with accession-specific regulation were sorted into seven clusters of similarly regulated genes by fuzzy *K*-means clustering, in which enriched GO categories were identified (Fig. 2*C*). The five largest clusters (K1 to K5) of contrasting response genes were characterized by stronger regulation in Bay-0 compared with Lp2-6. During submergence in Bay-0, the GO terms "rRNA processing" and "ribosome biogenesis" were strongly down-regulated and only marginally recovered upon desubmergence in cluster 1 (K1). In Lp2-6, these genes hardly responded to submergence and returned to their original values upon recovery. The same behavior was found in K2, however, with no recovery in Bay-0 but with a clear recovery response in Lp2-6. GO categories enriched in K2 were related to photosynthesis, light stimuli, and pigment biosynthesis. K4, the largest group, was characterized by strong up-regulation during submergence and little recovery response in Bay-0. However, in Lp2-6, gene induction during submergence was smaller and expression values approached their original control levels during recovery. Corresponding GO categories were related to ethylene and ABA signaling, senescence, autophagy, biotic defense, and oxidative stress.

Inability to Maintain ROS Homeostasis Hinders Recovery. Ribo-seq analyses strongly pointed toward oxidative stress and ROS metabolism as important recovery components. As fuzzy *K*-means plots revealed, both similarly and contrastingly responding genes are overrepresented in GO categories related to oxidative stress (Fig. 2*C* and *SI Appendix*, Fig. S3). During submergence, more of these transcripts were associated with ribosomes, with a further increase after 3 h of recovery. Since this trend was stronger in Bay-0, we investigated the hypothesis that Bay-0 experienced greater oxidative stress, thus hindering recovery.

ROS production was measured by assessing levels of the lipid peroxidation product malondialdehyde (MDA). After 5 d of submergence (0 h after desubmergence), shoot MDA levels were similar to levels in shoots from control nonsubmerged plants and not different between the accessions (Fig. 3*A*). During subsequent recovery, MDA levels sharply increased in the sensitive Bay-0 within 3 h, and continued to increase over the 3 d of recovery monitored. By contrast, MDA levels in Lp2-6 shoots remained much lower at all recovery time points. ROS production in intermediary leaves was directly quantified using electron paramagnetic resonance (EPR) spectroscopy, which facilitates radical species detection by combination with a spin trapping technique to prolong radical half-life. EPR revealed that ROS content in intermediary leaves under control conditions was close to the detection limit (Fig. 3*B*).

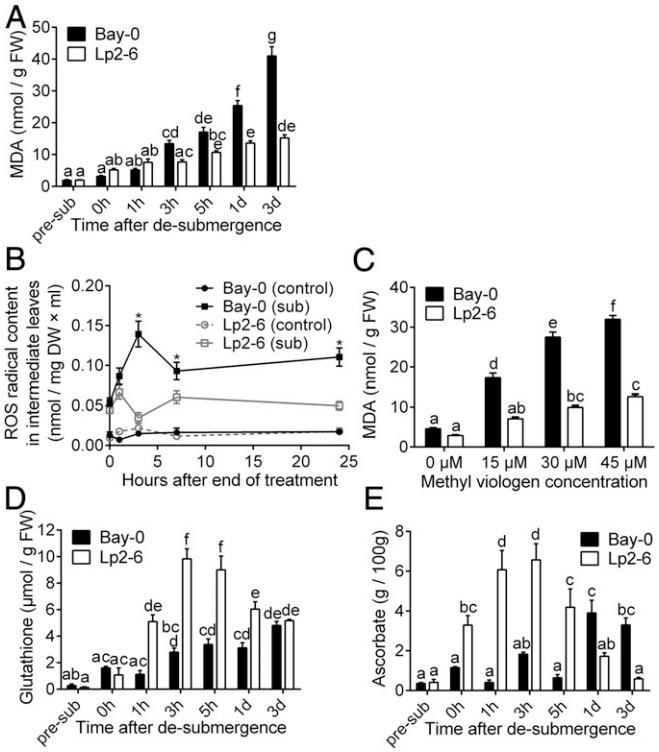

Fig. 3. Lp2-6 effectively contains oxidative stress resulting from excessive ROS during recovery. (*A*) Malondialdehyde content of Bay-0 and Lp2-6 rosettes before submergence (pre-sub), after 5 d of submergence (0h), and during subsequent recovery (n = 7). FW, fresh weight. (*B*) Electron paramagnetic resonance spectroscopy quantified ROS in Bay-0 and Lp2-6 intermediary leaves of control or recovering plants after 5 d of submergence (n = 30). Asterisks represent significant difference (P < 0.05) between submerged accessions at the specified time point. (*C*) MDA content of rosettes with varying concentrations of exogenously applied methyl viologen (n = 7). (*D* and *E*) Glutathione (*D*) and ascorbate (*E*) content in intermediary leaves recovering from 5 d of submergence (n = 3). Data represent mean ± SEM. In all panels except *B*, significant difference is denoted by different letters (P < 0.05, one- or two-way ANOVA with Tukey's multiple comparisons test).

Whereas ROS levels were comparable between the accessions at the end of 5 d of submergence, levels began to increase 1 h after desubmergence in both accessions. This indicated that ROS production is most pronounced following desubmergence. In Bay-0, ROS accumulation peaked at 3 h of recovery. Afterward, ROS levels dropped but remained relatively high until the last measurement time point of 24 h after desubmergence. ROS levels surged in Lp2-6 1 h after desubmergence, corresponding to concurrent slightly higher MDA production, but subsequently dropped and remained at significantly lower levels than Bay-0 at all subsequent time points. ROS were also measured on intermediary leaves from plants placed in darkness for 5 d followed by recovery in control light conditions (*SI Appendix*, Fig. S4*A*). In both accessions, despite higher ROS levels than control leaves after 5 d of darkness, there was no increase in the recovery period and ROS decreased to the same levels as control plants at 7 and 24 h of reillumination. Thus, the ROS burst and ROS content differences during recovery between the two accessions following desubmergence are linked to reoxygenation rather than reillumination.

The direct ROS measurements confirmed that recovery triggered greater ROS accumulation and associated damage in Bay-0. We therefore hypothesized that improved recovery in Lp2-6 is associated with higher oxidative stress tolerance. To assess this, nonsubmerged plants were sprayed with increasing concentrations of ROS-generating methyl viologen (26, 27). For all methyl viologen concentrations tested, Bay-0 had significantly higher MDA levels than Lp2-6, indicating higher ROS-mediated damage and sensitivity to oxidative stress (Fig. 3*C*). To determine whether higher oxidative stress tolerance of Lp2-6 could be a consequence of better ROS amelioration capacity, the antioxidants glutathione and ascorbate were quantified in intermediary leaves. After 5 d of submergence, ascorbate content was significantly higher in Lp2-6, but glutathione levels were similar to those of nonstressed plants in both accessions (Fig. 3 *D* and *E*). Starting from 1 h of recovery, both glutathione and ascorbate increased significantly in Lp2-6, and continued to increase compared with controls (pre-sub) up to 3 to 5 h after desubmergence. Although ascorbate levels increased in Bay-0, this was delayed compared with Lp2-6 (from 1 d of recovery onward).

Additionally, we looked for candidate accession-specific genes in the Ribo-seq dataset that could explain higher ROS production in Bay-0. We identified the plasma membrane-bound NADPH oxidase *RESPIRATORY BURST OXIDASE HOMOLOG D* (At5g46910) that catalyzes ROS production. Ribosome-associated transcript abundance of *RBOHD* increased during submergence in Bay-0, and recovery conditions further elevated *RBOHD* transcript abundance compared with a moderate induction in Lp2-6 (*SI Appendix*, Fig. S2*D*). This was further confirmed at the level of total transcript abundance by qRT-PCR in an independent experiment (*SI Appendix*, Fig. S4*B*).

To assess the physiological role of *RBOHD* and an associated ROS burst during recovery, the well-characterized *rbohD-3* loss-of-function mutant (28, 29) was investigated in comparison with its wild-type background Col-0, which is of intermediary submergence tolerance (18, 30). The *rbohD-3* mutant effectively limited ROS production during recovery, as discerned by extremely low MDA content in contrast to wild-type Col-0 plants (Fig. 4*A* and *SI Appendix*, Fig. S4*A*). However, despite the high MDA content (Fig. 4*A*), wild-type plants recovered from submergence better than *rbohD-3*, as reflected in higher chlorophyll content (Fig. 4*B*) and faster new leaf formation (Fig. 4*C* and *SI Appendix*, Fig. S4*C*).

The necessity of a transient ROS burst involving *RBOHD* upon desubmergence to initiate signaling might explain the slower recovery of *rbohD-3* mutants. Spraying plants with low concentrations of methyl viologen upon desubmergence retarded new leaf formation in Col-0 but not in *rbohD-3* plants, suggesting that limited ROS production might be beneficial to recovery (*SI Appendix*, Fig. S6). However, based on higher *RBOHD* transcript accumulation in Bay-0, we hypothesized that excessive and prolonged ROS production hinders recovery. To test this, the transient ROS burst observed upon desubmergence (3 and 1 h after desubmergence in Bay-0 and Lp2-6, respectively) was manipulated by chemical inhibition of *RBOH* activity. Rosettes were sprayed with the NADPH oxidase inhibitor diphenyleneiodonium (DPI) during the first hour after desubmergence. In Bay-0, DPI application significantly reduced MDA content during recovery (Fig. 4*D*). Furthermore, DPI boosted Bay-0 recovery compared with mock-sprayed plants (*SI Appendix*, Fig. S4*D*), as reflected in significantly higher chlorophyll content within 1 d of recovery (Fig. 4*E*) and faster new leaf development (Fig. 4*F*). For Lp2-6, which accumulated less ROS upon recovery, DPI application further reduced ROS production, as indicated by MDA content (Fig. 4*G*). MDA content in DPI-sprayed plants was low at all recovery time points, although slightly higher than levels in *rbohD-3*, whereas mock-sprayed plants had strong MDA accumulation up to 3 d of desubmergence. Even though the dampening of recovery by DPI on Lp2-6 was not as severe as in *rbohD-3* (*SI Appendix*, Fig. S4*E*), recovery was hindered in DPI-sprayed Lp2-6 plants, as indicated by lower chlorophyll content (Fig. 4*H*) and delayed production of new leaves (Fig. 4*I*).

These data demonstrate that excessive ROS accumulation limits recovery, whereas limited and controlled ROS production soon after desubmergence is beneficial for recovery. In Bay-0, DPI application likely dampened the otherwise excessive ROS

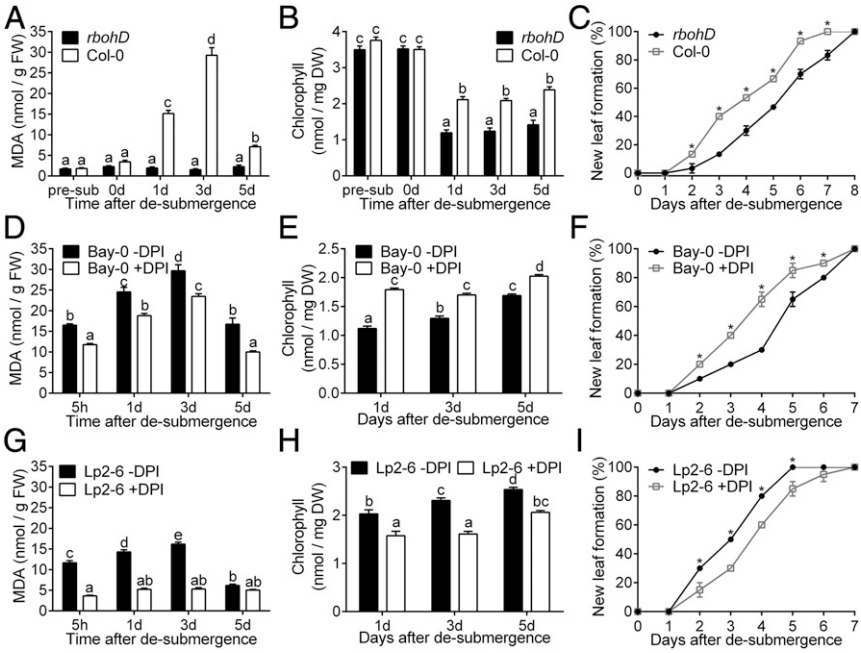

Fig. 4. Postsubmergence ROS formation mediated through *RBOHD* regulates recovery. (*A–C*) MDA content ($n = 12$) (*A*), chlorophyll content ($n = 12$) (*B*), and new leaf formation (*C*) of *rbohD-3* and Col-0 ($n = 30$) rosettes during recovery following 5 d of submergence. (*D–F*) MDA content ($n = 20$) (*D*), chlorophyll content ($n = 20$) (*E*), and new leaf formation ($n = 20$) (*F*) of Bay-0 plants with or without diphenyleneiodonium application upon desubmergence. (*G–I*) MDA content ($n = 20$) (*G*), chlorophyll content ($n = 20$) (*H*), and new leaf formation ($n = 20$) (*I*) during recovery of Lp2-6 plants sprayed with or without DPI upon desubmergence. Data represent mean ± SEM. Asterisks represent a significant difference between the two accessions at the specified time point ($P < 0.05$, two-way ANOVA with Sidak's multiple comparisons test). Significant difference is denoted by different letters ($P < 0.05$, two-way ANOVA with Tukey's multiple comparisons test).

formed upon desubmergence, thus improving recovery. However, Lp2-6 recovery was hampered when ROS levels were significantly reduced over the recovery time course. We conclude that a fine-tuned balance between production and scavenging of ROS generated by RBOHD and possibly other NADPH oxidases is critical for recovery of leaf formation and ultimately fecundity following desubmergence.

Dehydration Stress Upon Desubmergence Hampers Recovery. Accession-specific DEGs were also enriched for GO categories associated with dehydration: ABA response and senescence (Fig. 2*C*). Dehydration and senescence were clearly visible during recovery, and these symptoms were more severe in Bay-0 (Fig. 1*A*). To assess leaf water management during recovery, relative water content (RWC) was measured in intermediary leaves following desubmergence (Fig. 5*A*). RWC dropped significantly in both accessions 3 h after desubmergence, although Lp2-6 retained higher water status. RWC values above 70% were maintained at subsequent time points by Lp2-6, while values dropped below 65% by 3 h and did not recover in Bay-0. A similar trend was observed in water loss assays in detached desubmerged shoots over a 6-h period. In both accessions, in the first hour after separation from the root, a steep increase in water loss was observed in detached shoots (Fig. 5*B*). However, water loss at all subsequent time points was significantly lower in Lp2-6.

As rate of water loss is closely linked to stomatal conductance, we investigated whether the differences in dehydration response between the accessions were related to stomatal traits. Stomatal size and density were not significantly different between the two accessions (*SI Appendix*, Fig. S1 *E* and *F*). However, stomatal aperture following desubmergence differed between Bay-0 and Lp2-6. While most stomata were partially open in both accessions an hour after desubmergence (Fig. 5*C*), stomatal aperture values further decreased in Lp2-6 and remained low up to 6 h after desubmergence, indicating stomatal closure. By contrast, Bay-0 stomata reopened by 3 h and remained open at 6 h after desubmergence, as indicated by higher stomatal aperture values. In addition to the stomata, the cuticle is also implicated in regulating plant water status. However, the abundance of ribosome-associated transcripts of cuticle-associated genes was not different between the two accessions during submergence or recovery (*SI Appendix*, Fig. S7).

Stomatal aperture regulation in response to drought signals is primarily controlled by ABA, supported by appearance of the "response to ABA" GO category (Fig. 2*C* and *SI Appendix*, Fig. S3). To examine stomatal responsiveness to exogenous ABA in the two accessions, abaxial epidermal peels from nonstressed plants were incubated in varying ABA concentrations (Fig. 5*D*). Lp2-6 was more sensitive to ABA, with significantly smaller stomatal apertures under 50 and 100 μM ABA compared with Bay-0. To determine if differences in ABA content contributed to the contrasting stomatal aperture response in Bay-0 and Lp2-6, ABA levels were measured in intermediary leaves after desubmergence and during the corresponding circadian light time points (Fig. 5*E*). Average ABA content in Bay-0 was higher after 5 d of submergence (0 h of desubmergence) and at all subsequent recovery time points up to 3 d of recovery. Since the ABA measurements did not reconcile with the role of ABA as a positive regulator of stomatal closure, we explored the data for desubmergence-associated signals that might antagonize ABA action.

Ethylene Accelerates Dehydration and Senescence During Recovery in Bay-0 Mediated by *SAG113* and *ORE1*. The Ribo-seq data revealed accession-specific genes in the "ethylene-activated signaling pathway" (Fig. 2*C*). To further investigate the role of ethylene in the differential submergence recovery responses of the two accessions, whole-plant ethylene emission was measured. Ethylene production was significantly higher in Bay-0 than in Lp2-6 after 5 d of submergence (0 h of desubmergence), and this trend persisted 1 h and 1 d after desubmergence (Fig. 6*A*). Ethylene production in

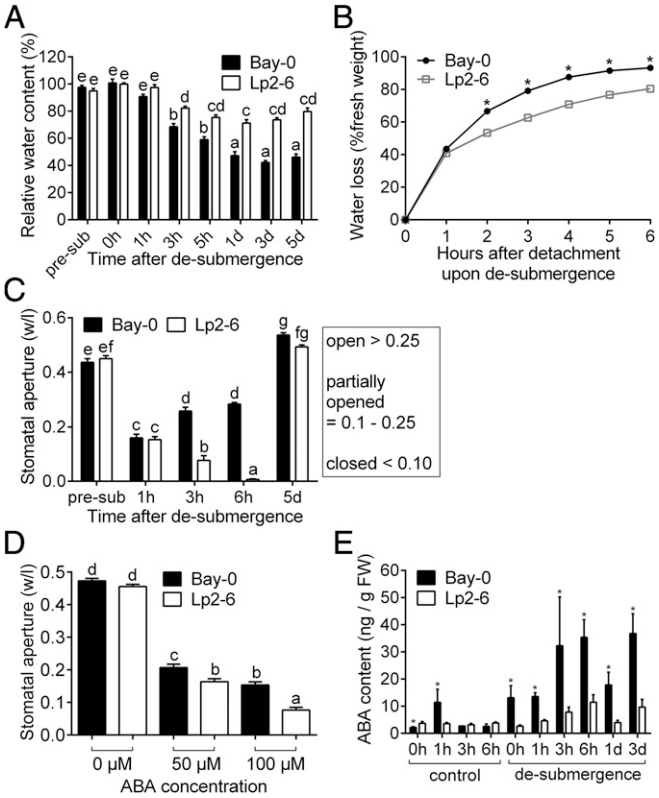

Fig. 5. Higher desiccation stress in Bay-0 corresponds to earlier stomatal opening during recovery. (*A*) Relative water content in intermediary leaves before submergence (pre-sub), after 5 d of submergence (0h), and subsequent recovery time points (n = 15). (*B*) Hourly water loss of 10-leaf-stage rosettes after detachment from roots immediately upon desubmergence (0 h) compared with the initial fresh weight (n = 30). (*C*) Stomatal width aperture (based on width/length ratio) measured using stomatal imprints on the adaxial side of intermediary leaves (n = 85 to 227) of plants before treatment (pre-sub), and subsequent recovery time points. (*D*) Stomatal aperture of epidermal peels from intermediary leaves of plants grown under control conditions and incubated in 0, 50, or 100 μM ABA (n = 180). (*E*) ABA quantification in intermediary leaves of Bay-0 and Lp2-6 recovering from 5 d of submergence and corresponding controls (n = 3). Data represent mean ± SEM. Different letters represent significant difference, and asterisks represent significant differences between the accessions at the specified time point (P < 0.05; *B*, two-way ANOVA with Tukey's multiple comparisons test; *E*, one-way ANOVA with planned comparisons on log-transformed data).

Lp2-6 was almost half that in Bay-0. To investigate whether this ethylene was causal to the stomatal response and plant performance, as reflected in higher chlorophyll loss in Bay-0 during recovery, ethylene action was blocked using 1-methylcyclopropene (1-MCP). Treatment of Bay-0 plants with 1-MCP following desubmergence strongly reduced the number of open stomata (Fig. 6*B*) and decline in chlorophyll content (Fig. 6*C*). We next explored the Ribo-seq dataset for genes that might mediate the ethylene effect on stomatal behavior and chlorophyll loss during recovery. Among the accession-specific genes, we identified two previously confirmed targets of the transcription factor EIN3, a positive regulator of ethylene signaling (31, 32): *SENESCENCE ASSOCIATED GENE113* (At5g59220) and the transcription factor *NAC DOMAIN CONTAINING PROTEIN6*/*ORE1*/*ORESARA1* (*ANAC092*/*NAC2*/*NAC6*; At5g39610).

Both *SAG113* and *ORE1* were identified as accession-specific genes with increased ribosome-associated transcript abundance in Bay-0 during submergence and 3 h of recovery, whereas Lp2-6 showed low induction of these transcripts. This trend was confirmed using qRT-PCR in an independent experiment assessing total *SAG113* and *ORE1* transcript abundance (Fig. 7 *A* and *B*). *SAG113* encodes a protein phosphatase 2C implicated in the inhibition of stomatal closure to accelerate water loss and senescence in *Arabidopsis* leaves (33, 34). *ORE1* has been previously characterized as a positive regulator of leaf senescence (35–37). In accordance with their identity as EIN3 targets, 1-MCP treatment of Bay-0 following desubmergence significantly repressed *ORE1* and *SAG113* transcript abundance increase during recovery (Fig. 7 *C* and *D*). Although 1-MCP suppressed the desubmergence-promoted transcript accumulation, both *ORE1* and *SAG113* are also reported to be ABA-inducible (33, 38). However, application of an ABA antagonist (AA1) (39) significantly suppressed the desubmergence-induced increase in transcript abundance of *SAG113* only (*SI Appendix*, Fig. S5). Accordingly, AA1-treated plants had a higher percentage of closed stomata, corresponding to the role of *SAG113* in stomatal closure of senescing leaves (*SI Appendix*, Fig. S5*E*). Effectiveness of the ABA inhibitory action of AA1 was confirmed by rescuing ABA-induced inhibition of seed germination (*SI Appendix*, Fig. S5*F*) and dark-induced senescence, as described by ref. 39, and qRT-PCR of the ABA-regulated genes *RD29B* and *RD22* (*SI Appendix*, Fig. S5 *C* and *D*).

Evaluation of a previously characterized knockout mutant for *SAG113* (33, 34) revealed an improved recovery phenotype (Fig. 7*E*) with significantly fewer closed stomata at 3 and 6 h after desubmergence compared with the wild-type Col-0, correlating with significantly reduced water loss (Fig. 7 *G* and *H*). Loss-of-function *ore1* mutants (35) had less visible leaf chlorosis (Fig. 7*F*) and significantly higher chlorophyll content after 5 d of recovery than wild-type Col-0 plants (Fig. 7*I*). In conclusion, *SAG113*, induced by the higher ethylene production and ABA levels in Bay-0, contributes to premature stomatal opening and subsequent dehydration. Simultaneously, higher ethylene production in Bay-0 was responsible for *ORE1* induction leading to senescence, as reflected in higher chlorophyll breakdown.

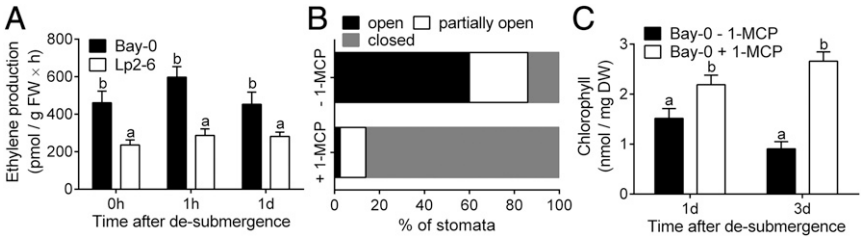

Fig. 6. Dehydration and accelerated senescence in Bay-0 upon desubmergence is linked to higher ethylene evolution during recovery. (*A*) Ethylene emissions from Bay-0 and Lp2-6 shoots after desubmergence (n = 4 or 5). (*B*) Stomatal classification at 3 or 6 h after desubmergence of Bay-0 plants treated with or without the ethylene perception inhibitor 1-MCP (n = 280 to 300). (*C*) Chlorophyll content in whole rosettes of Bay-0 treated with or without 1-MCP (n = 5 or 6). 1-MCP treatment was imposed immediately upon desubmergence. Data represent mean ± SEM. Different letters represent significant difference (P < 0.05, two-way ANOVA with Tukey's multiple comparisons test).

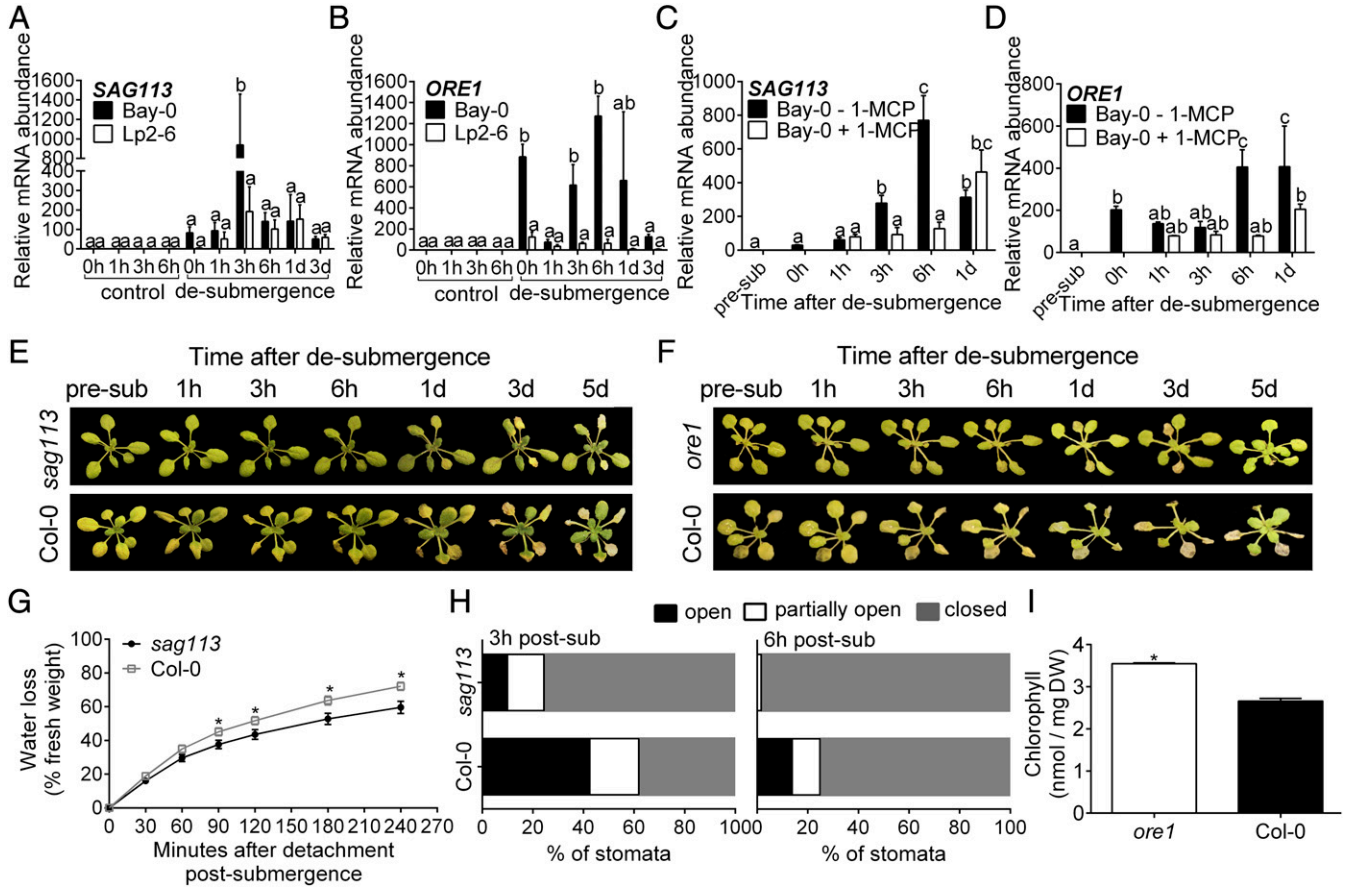

Fig. 7. Ethylene-mediated dehydration and senescence in Bay-0 postsubmergence link to the induction of *SAG113* inhibiting stomatal closure and *ORE1* promoting chlorophyll breakdown. (*A* and *B*) Relative mRNA abundance of *SAG113* (*A*) and *ORE1* (*B*) measured by qRT-PCR in Bay-0 and Lp2-6 intermediary leaves following desubmergence after 5 d of submergence ($n = 3$ biological replicates). (*C* and *D*) Relative mRNA abundance of *SAG113* (*C*) and *ORE1* (*D*) measured by qRT-PCR in intermediary leaves of Bay-0 plants treated with and without 1-MCP ($n = 3$ or 4 biological replicates). (*E* and *F*) Representative images of *sag113* (*E*) and *ore1* (*F*) mutants during recovery after 4 d of submergence compared with wild-type Col-0. (*G*) Water loss in *sag113* and Col-0 after detachment from roots upon desubmergence compared with the initial fresh weight ($n = 4$). (*H*) Stomatal classification at 3 and 6 h after desubmergence for *sag113* and Col-0 submerged for 4 d ($n = 120–180$). (*I*) Chlorophyll content in whole rosettes of *ore1* and Col-0 after 5 d of recovery following 4 d of submergence ($n = 3$). Data represent mean ± SEM. Different letters represent significant difference, and asterisks represent significant difference between genotypes at the specified time point ($P < 0.05$, two-way ANOVA with Tukey's multiple comparisons test).

Discussion

Timely recovery following stress exposure is critical for plant survival. Flooding severely reduces light intensity and gas exchange, and subsequent effects on respiration and photosynthesis cause severe energy and carbon imbalances (2). Floodwater retreat poses new stress conditions, as low light- and hypoxia-acclimated plant tissues encounter terrestrial conditions again. Here we exploited two *Arabidopsis* accessions in which differences in submergence tolerance were primarily due to distinctions in submergence recovery. This system revealed that superior recovery after desubmergence is an important aspect of submergence tolerance linked to reproductive output and thus plant fitness (Fig. 1*C*). Using these accessions, we sought to identify molecular and physiological processes and regulatory components influencing recovery.

It is generally accepted that the transition back to reilluminated and reoxygenated conditions results in a transient ROS burst in recovering tissues due to reactivation of photosynthetic and mitochondrial electron transport promoting excessive electron and proton leakage (40–42). Reoxygenation led to increased ROS production in both accessions, but sensitive Bay-0 was unable to control prolonged and excessive ROS production during recovery. This could explain the severe photoinhibition (Fig. 1*F*) and hindered starch replenishment in this accession (Fig. 1*G*) during submergence recovery. ROS production differences between the two accessions corresponded to higher *RBOHD* transcript abundance during recovery in Bay-0. Counterintuitively, significantly reducing postsubmergence ROS generation through genetic (*rbohD-3*) or pharmacological means (DPI application in Lp2-6) worsened recovery. Although excessive ROS are damaging, controlled ROS production via RBOHD might be required for stress signaling during submergence recovery.

ROS production has been previously implicated in hypoxia signaling (43, 44). *RBOHD* is an *Arabidopsis* core hypoxia gene (45, 46), and a transient RBOHD-mediated ROS burst during hypoxia was found to be essential for induction of genes required for hypoxia acclimation (anaerobic metabolism) and seedling survival (44). Pretreatment of *Arabidopsis* seedlings with DPI before hypoxia reduced core response gene up-regulation and limited survival (43). *RBOHD* is also a candidate gene within a quantitative trait locus conferring submergence tolerance in 10- to 12-leaf-stage *Arabidopsis* (47). Our results demonstrate that *RBOHD* also has an essential role in submergence recovery. In Lp2-6, higher oxidative stress tolerance was linked to restricted ROS accumulation within 1 h of desubmergence and a significant increase in antioxidant status (Fig. 3 *D* and *E*). Clearly, maintenance of a delicate balance of ROS and antioxidants is critical to

cellular homeostasis. While controlled ROS production is essential, it needs to be countered by an effective antioxidant defense system that can manage excessive ROS accumulation and associated damage. The recovery signals regulating *RBOHD* are unclear, but it is likely to be under hormonal control.

Our work also highlighted dehydration stress and accelerated senescence as deterrents to recovery. Plants recovering from flooding often experience physiological drought due to impaired root hydraulics and/or leaf water loss (9, 13, 48, 49). Tolerant Lp2-6 rosettes regulated water loss following desubmergence more effectively than Bay-0. The inferior hydration status of Bay-0 correlated with earlier stomatal reopening 3 h following desubmergence. The smaller stomatal apertures of Lp2-6 most probably counteracted dehydration during recovery. The Ribo-seq data and hormone measurements indicated a stronger ABA response in Bay-0, conflicting with the role of ABA in promoting stomatal closure in response to drought signals. However, the Ribo-seq data also revealed a possible role for ethylene signaling in mediating recovery differences between the accessions (Fig. 2*C*). Ethylene is a senescence-promoting hormone that can antagonize ABA action on stomatal closure (50). Elevated ethylene production following desubmergence in Bay-0 corresponded to both an earlier stomatal reopening and greater chlorophyll loss, since chemical inhibition of ethylene signaling during recovery reversed both traits. We suggest that ethylene action is mediated through the EIN3 target genes *SAG113* and *ORE1*, identified as accession-specific regulated genes with higher transcript abundance in Bay-0 during recovery. Accordingly, knockout mutants in the Col-0 wild-type background, with intermediary submergence tolerance (18), showed improved recovery following desubmergence, associated with improved water loss and reduced senescence. Although previous work on *Arabidopsis* seedlings recovering from anoxic stress (8) revealed that ethylene is beneficial for recovery, our data indicate a negative role for ethylene in submergence recovery. Since 1-aminocyclopropane-1-carboxylic acid (ACC) conversion to ethylene requires oxygen, ethylene production is limited by anoxic conditions during prolonged submergence (51). Higher ethylene production in Bay-0 upon desubmergence might imply more ACC accumulation during submergence. Expression of several ACC synthase genes was indeed higher in Bay-0, either during submergence or recovery (*SI Appendix*, Fig. S8). Upon reoxygenation, ethylene formation mediated by ACC synthase and ACC oxidase enzymes may accelerate dehydration and senescence by inducing *ORE1* and *SAG113*.

The increase in *SAG113* transcript abundance following desubmergence was reduced upon application of an ABA antagonist, indicating ABA regulation of this gene (*SI Appendix*, Fig. S5*A*). This implied that high ABA levels in Bay-0 would promote stomatal opening via *SAG113* up-regulation, rather than closure, which appears counterintuitive. However, this may reflect interplay between ABA and ethylene signaling pathways. The induction of *SAG113* in Bay-0 could be a means to accelerate senescence of older leaves to remobilize resources to younger leaves, and possibly meristematic regions for new leaf development. How ethylene and ABA interactions influence recovery is an interesting area for future research.

Based on our findings, we propose a signaling network that regulates submergence recovery. Following desubmergence, dehydration caused by reduced root function and reoxygenation generates the submergence recovery signals ROS, ABA, and ethylene that elicit downstream signaling pathways regulating various aspects of recovery (Fig. 8). Recovery signaling requires *RBOHD*-mediated ROS production, but this must be transient to prevent subsequent oxidative damage and photoinhibition. ABA and ethylene signaling likely interact to control stomatal opening, dehydration, and senescence through regulation of genes such as *SAG113* and *ORE1*. This work provides key new insights into the highly regulated processes following desubmergence that limit recovery of Bay-0 and bolster survival of Lp2-6, emphasizing selection on mechanisms enhancing the return to homeostasis.

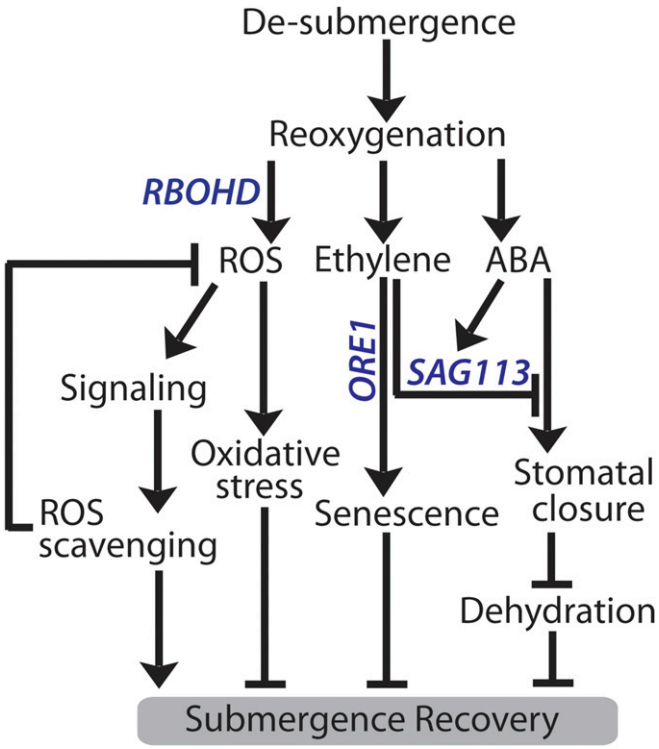

Fig. 8. Signaling network mediating postsubmergence recovery. Following prolonged submergence, the shift to a normoxic environment generates the postsubmergence signals ROS, ethylene, and ABA. A ROS burst upon reoxygenation occurs due to reduced scavenging and increased production in Bay-0 from several sources, including *RBOHD* activity. While excessive ROS accumulation is detrimental and can cause cellular damage, ROS-mediated signaling is required to trigger downstream processes that benefit recovery, including enhanced antioxidant capacity for ROS homeostasis. Signals triggering *RBOHD* induction following desubmergence are unclear, but hormonal control is most likely involved. Recovering plants experience physiological drought due to reduced root conductance, resulting in increased ABA levels postsubmergence which can regulate stomatal movements to offset excessive water loss. High ethylene production in Bay-0 caused by ACC oxidation upon reaeration can counter drought-induced stomatal closure via induction of the protein phosphatase 2C *SAG113*, accelerating water loss and senescence. Higher transcript abundance of *SAG113* in Bay-0 is also positively regulated by ABA, and could be a means to speed up water loss and senescence in older leaves. Ethylene also accelerates chlorophyll breakdown via the NAC transcription factor *ORE1*. The timing of stomatal reopening during recovery is critical for balancing water loss with CO_2 assimilation, and is likely regulated by postsubmergence ethylene–ABA dynamics and signaling interactions.

Materials and Methods

Plant Growth and Submergence Treatment. *Arabidopsis* seeds were obtained from the Nottingham *Arabidopsis* Stock Centre or received from the listed individual: Bay-0 (accession CS22633), Lp2-6 (accession CS22595), Col-0, *rbohD-3* (N9555, containing a single dSpm transposon insertion, received from Ron Mittler, University of North Texas, Denton, TX) (28), *sag113* (SALK_142672C, containing a T-DNA insertion) (34), and *ore1* (SALK_090154, containing a T-DNA insertion) (35). All mutants were in the Col-0 wild-type background and genotyped to confirm the presence of the insertion (*SI Appendix*, Table S1). Seeds were sown on a 1:2 part soil:perlite mixture, stratified (4 d in the dark, 4 °C), and grown under short-day light conditions [9 h light, 20 °C, 180 $\mu mol \cdot m^{-2} \cdot s^{-1}$ photosynthetically active radiation (PAR), 70% relative humidity (RH)]. At 2-leaf stage, seedlings were transplanted into pots with the same soil mixture covered with a mesh. For submergence, disinfected tubs were filled with water for overnight temperature equilibrium to 20 °C. Homogeneous 10-leaf-stage plants were submerged at 10:00 AM (2 h after the start of the photoperiod) at 20-cm water depth in a dark 20 °C temperature-controlled climate room. After 5 d of submergence, desubmerged plants were re-placed under normal growth conditions to follow postsubmergence recovery.

Chlorophyll and Dry Weight. Chlorophyll was extracted from whole rosettes or only intermediary leaves with 96% (vol/vol) DMSO dark-incubated at 65 °C and cooled to room temperature. Absorbance at 664, 647, and 750 nm was measured with a spectrophotometer plate reader (Synergy HT Multi-Detection Microplate Reader; BioTek Instruments). Chlorophyll a and b concentrations were calculated following the equations of ref. 52. Rosettes and leaves were dried in a 70 °C oven for 2 d for dry weight measurements.

Seed Yield. Control and desubmerged plants grown under short-day conditions were watered daily until the terminal bud stopped flowering, and removed from high humidity conditions for drying until all siliques turned brown. Seeds were collected from individual plants and weighed.

Shoot and Root Grafting. Grafting methods were based on ref. 53. Sterilized seeds sown on 1/2 Murashige and Skoog plates containing 1% (wt/vol) agar and 0.5% (wt/vol) sucrose were stratified (3 d in the dark, 4 °C) and grown under short-day light conditions for 6 d. Shoots and roots were grafted in a new 1/2 MS plate and vertically grown for 10 d. Adventitious roots were excised before transplanting seedlings into mesh-covered pots containing 1:2 parts soil:perlite. Plants were grown under short-day conditions until the 10-leaf stage for 5 d of dark submergence.

Chlorophyll Fluorescence Measurements. F_v/F_m was measured in intermediary leaves. Plants were dark-acclimated for 10 min before using a PAM-2000 Portable Chlorophyll Fluorometer (Heinz Walz). The sensor was placed at a 5-mm distance from the leaf. Leaves with an F_v/F_m below detection level were marked as dead.

Starch Quantification. Starch levels were measured in whole rosettes using a commercial starch determination kit (Boehringer) following the manufacturer's protocol.

Ribo-Seq Library Construction. Four intermediary leaves of each rosette submerged for 5 d were frozen in liquid nitrogen at 0 h (10:00 AM, immediately upon desubmergence) and 3 h of air and light recovery. Intermediary leaves of 10-leaf-stage control plants were harvested at 0 h. Five milliliters of packed tissue was used to isolate ribosome-protected fragments. Ribo-seq libraries were prepared following the methods of refs. 54–56. Ribo-seq libraries were multiplexed with two samples in each lane. Libraries were sequenced with a HiSeq 2500 (Illumina) sequencer with 50-bp single-end reading. Bioinformatic analyses are described in *SI Appendix, SI Materials and Methods*.

Malondialdehyde Measurements. MDA was quantified using a colorimetric method modified from ref. 57. Leaves were pulverized in 80% (vol/vol) ethanol, and the supernatant was mixed with a reactant mixture of 0.65% (wt/vol) thiobarbituric acid and 20% (wt/vol) trichloroacetic acid. After a 30-min incubation at 95 °C, absorbance was measured at 532 and 600 nm with a spectrophotometer plate reader.

Electron Paramagnetic Resonance Spectroscopy. Intermediary leaves were harvested for each treatment (control, dark, and recovery following submergence) and incubated with a TMT-H (1-hydroxy-4-isobutyramido-2,2,6,6-tetramethyl-piperidinium) spin probe. The supernatant was measured on a Bruker Elexsys E500 spectrometer. Further details are listed in *SI Appendix*.

Methyl Viologen Application. Plants were sprayed with methyl viologen (0, 15, 30, 45 μM) containing 0.1% (vol/vol) Tween-20 1 d before harvesting. Control plants were sprayed with 0.1% (vol/vol) Tween-20 to account for detergent effects. Plants were sprayed three times during the day, each time with 1 mL of solution.

Antioxidant Measurements. Glutathione was measured with a Promega GSH-Glo Glutathione Assay Kit, following the manufacturer's procedure, using 25 to 50 mg of fresh tissue. Ascorbate was measured using a kit from Megazyme (K-ASCO 01/14), following the microplate assay procedure with 50 to 75 mg of fresh tissue.

Scoring New Leaf Development. Leaves were scored as newly formed during recovery from submergence when emergence from the shoot meristem was clearly visible.

Application of Chemical Inhibitors of *RBOHD*, ABA, and Ethylene. Upon desubmergence, shoots were sprayed with 400 μL of 200 μM DPI (Sigma-Aldrich) containing 0.1% Tween-20 or 100 μM AA1 ($C_{18}H_{23}N_5OS_2$; F0544-0152; Life Chemicals) containing 0.1% (vol/vol) DMSO. Control plants were also sprayed with mock solution containing only 0.1% (vol/vol) Tween-20 or DMSO. Plants were sprayed again with 200 μL of DPI or AA1 30 min and 1 h after the first application. For 1-MCP gassing, plants placed in glass desiccators (22.5-L volume) were gassed with 5 ppm 1-MCP (Rohm and Haas). Control plants were placed in a separate desiccator to control for humidity effects. After 15 min, plants were re-placed under normal growth conditions. 1-MCP (5 ppm) was reapplied to the plants every 4 h during the first day after desubmergence.

Relative Water Content. Four intermediary leaves per rosette were detached and fresh weight was recorded. Leaves were saturated in water, and saturated weight was measured after 24 h. Leaves were dried in an 80 °C oven for 2 d before measuring dry weight. Relative water content was calculated by [(fresh weight − dry weight)/(saturated weight − dry weight)] × 100.

Rapid Dehydration Assays. Excised rosettes were weighed hourly up to 8 h after cutting and placed in a controlled environment at ambient room temperature (22.3 °C, 12 $\mu mol \cdot m^{-2} \cdot s^{-1}$ PAR, 63% RH).

Stomatal Imprints. Adaxial sides of leaves were imprinted using a silicone-based dental impression kit (Coltène/Whaledent PRESIDENT light body ISO 4823). Leaves were gently pressed onto the silicone mixture and removed after solidification. Transparent nail polish was thinly brushed onto the impression and air-dried. Stomata were viewed on the nail polish impression under an Olympus BX50WI microscope. Stomatal aperture was reported as width (w) divided by length (l) and classified as open (w/l > 0.25), partially open (w/l = 0.1 to 0.25), or closed (w/l = 0 to 0.10). Stomatal measurement immediately upon desubmergence after 5 d of submergence was excluded, since the mechanical stress of blotting wet leaves forced stomata to open in Lp2-6.

ABA Treatment in Epidermal Peels. Epidermal peels were obtained from intermediary leaves of 10-leaf-stage rosettes 2 h after the light period began. The adaxial side of the leaf was placed on sticky tape, and the petiole was ripped toward the leaf to obtain a transparent film of the abaxial side. Epidermal peels were placed in potassium stomata-opening buffer [50 mM KCl + 10 mM MES buffer (2-(N-morpholino)ethanesulfonic acid), pH 6.15] for 3 h under high light (180 $\mu mol \cdot m^{-2} \cdot s^{-1}$ PAR) and incubated for 1 h in stomata-closing buffer (2.5 μM $CaCl_2$ + 10 mM Mes, pH 6.15) containing 0, 50, or 100 μM ABA. Stomata on the epidermal peels were viewed under a microscope.

ABA Extraction and Quantification. Intermediary leaves (60 to 100 mg) were harvested after desubmergence, and control samples were harvested at the same time. ABA was extracted as described in ref. 58, and quantified by liquid chromatography-mass spectrometry (LC-MS) on a Varian 320 Triple Quad LC-MS/MS. ABA levels were quantified from the peak area of each sample compared with the internal standard, normalized by fresh weight.

Ethylene Emission Measurements. Ethylene production was measured based on ref. 51. Two shoots were placed in a 10-mL glass vial and entrapped ethylene was allowed to escape for 2 min before tightly sealing the vials. After a 5-h dark incubation, ethylene was collected with a 1-mL injection needle and measured by gas chromatography (Syntech).

RNA Extraction and Quantitative Real-Time qPCR. Total RNA was extracted following the Qiagen RNeasy Mini Kit protocol. For qRT-PCR, single-stranded cDNA was synthesized from 1 μg RNA using random hexamer primers (Invitrogen). qRT-PCR was performed on an Applied Biosystems ViiA 7 Real-Time PCR System (Thermo Fisher Scientific) with SYBR Green Master Mix (Bio-Rad). Primers used are listed in *SI Appendix*, Table S2. Relative transcript abundance was calculated using the comparative $2^{-\Delta\Delta CT}$ method (59) normalized to *ACTIN2*.

ACKNOWLEDGMENTS. At Utrecht University, we thank Rob Welschen for managing the growth facilities, Emilie Reinen and Zeguang Liu for genotyping mutant lines, Yorrit van de Kaa for seed harvesting, and Sven Teurlincx and Ankie Ammerlaan for experimental assistance. We appreciate Timo Staffel at the University of Kiel for assisting with plant growth for EPR measurements. We thank Thomas Girke of the University of California, Riverside for guidance on the Ribo-seq workflow in R/Bioconductor. This work was supported by grants (to R.S.) from the Netherlands Organisation for Scientific Research (NWO 016.VIDI.171.006 and NWO-VENI 863.12.013) and grants (to J.B.-S.) from the US National Science Foundation (MCB-1021969) and the US Department of Agriculture National Institute of Food and Agriculture Hatch program. E.Y. was supported by a PhD scholarship from Utrecht University.

1. Bailey-Serres J, Lee SC, Brinton E (2012) Waterproofing crops: Effective flooding survival strategies. *Plant Physiol* 160:1698–1709.
2. Voesenek LACJ, Bailey-Serres J (2015) Flood adaptive traits and processes: An overview. *New Phytol* 206:57–73.
3. Hirabayashi Y, et al. (2013) Global flood risk under climate change. *Nat Clim Chang* 3: 816–821.
4. Jackson MB (1985) Ethylene and responses of plants to soil waterlogging and submergence. *Annu Rev Plant Physiol* 36:145–174.
5. Armstrong W (1980) Aeration in higher plants. *Adv Bot Res* 7:225–332.
6. Maurel C, Simonneau T, Sutka M (2010) The significance of roots as hydraulic rheostats. *J Exp Bot* 61:3191–3198.
7. Tamang BG, Magliozzi JO, Maroof MAS, Fukao T (2014) Physiological and transcriptomic characterization of submergence and reoxygenation responses in soybean seedlings. *Plant Cell Environ* 37:2350–2365.
8. Tsai KJ, Chou SJ, Shih MC (2014) Ethylene plays an essential role in the recovery of *Arabidopsis* during post-anaerobiosis reoxygenation. *Plant Cell Environ* 37: 2391–2405.
9. Fukao T, Yeung E, Bailey-Serres J (2011) The submergence tolerance regulator SUB1A mediates crosstalk between submergence and drought tolerance in rice. *Plant Cell* 23: 412–427.
10. Ella ES, Kawano N, Ito O (2003) Importance of active oxygen-scavenging system in the recovery of rice seedlings after submergence. *Plant Sci* 165:85–93.
11. Biemelt S, Keetman U, Albrecht G (1998) Re-aeration following hypoxia or anoxia leads to activation of the antioxidative defense system in roots of wheat seedlings. *Plant Physiol* 116:651–658.
12. Monk LS, Fagerstedt KV, Crawford RM (1987) Superoxide dismutase as an anaerobic polypeptide: A key factor in recovery from oxygen deprivation in *Iris pseudacorus*? *Plant Physiol* 85:1016–1020.
13. Alpuerto JB, Hussain RMF, Fukao T (2016) The key regulator of submergence tolerance, *SUB1A*, promotes photosynthetic and metabolic recovery from submergence damage in rice leaves. *Plant Cell Environ* 39:672–684.
14. Khan MN, Komatsu S (2016) Characterization of post-flooding recovery-responsive enzymes in soybean root and hypocotyl. *J Plant Biol* 59:478–487.
15. Ye XQ, et al. (2016) Submergence causes similar carbohydrate starvation but faster post-stress recovery than darkness in *Alternanthera philoxeroides* plants. *PLoS One* 11:e0165193.
16. Yuan L, et al. (2017) Jasmonate regulates plant responses to reoxygenation through activation of antioxidant synthesis. *Plant Physiol* 173:1864–1880.
17. Tsai KJ, Lin CY, Ting CY, Shih MC (2016) Ethylene-regulated glutamate dehydrogenase fine-tunes metabolism during anoxia-reoxygenation. *Plant Physiol* 172: 1548–1562.
18. Vashisht D, et al. (2011) Natural variation of submergence tolerance among *Arabidopsis thaliana* accessions. *New Phytol* 190:299–310.
19. Ingolia NT, Ghaemmaghami S, Newman JRS, Weissman JS (2009) Genome-wide analysis in vivo of translation with nucleotide resolution using ribosome profiling. *Science* 324:218–223.
20. Ingolia NT (2014) Ribosome profiling: New views of translation, from single codons to genome scale. *Nat Rev Genet* 15:205–213.
21. Juntawong P, Bailey-Serres J (2012) Dynamic light regulation of translation status in *Arabidopsis thaliana*. *Front Plant Sci* 3:66.
22. Branco-Price C, Kaiser KA, Jang CJH, Larive CK, Bailey-Serres J (2008) Selective mRNA translation coordinates energetic and metabolic adjustments to cellular oxygen deprivation and reoxygenation in *Arabidopsis thaliana*. *Plant J* 56:743–755.
23. Benina M, Ribeiro DM, Gechev TS, Mueller-Roeber B, Schippers JHM (2015) A cell type-specific view on the translation of mRNAs from ROS-responsive genes upon paraquat treatment of *Arabidopsis thaliana* leaves. *Plant Cell Environ* 38:349–363.
24. Cheng MC, et al. (2015) Increased glutathione contributes to stress tolerance and global translational changes in *Arabidopsis*. *Plant J* 83:926–939.
25. Sorenson R, Bailey-Serres J (2014) Selective mRNA translation tailors low oxygen energetics. *Low-Oxygen Stress in Plants*, eds van Dongen JT, Licausi F (Springer, Vienna), pp 95–115.
26. Dodge AD, Harris N (1970) The mode of action of paraquat and diquat. *Biochem J* 118:43P–44P.
27. Bus JS, Aust SD, Gibson JE (1974) Superoxide- and singlet oxygen-catalyzed lipid peroxidation as a possible mechanism for paraquat (methyl viologen) toxicity. *Biochem Biophys Res Commun* 58:749–755.
28. Torres MA, Dangl JL, Jones JDG (2002) *Arabidopsis* gp91phox homologues AtrbohD and AtrbohF are required for accumulation of reactive oxygen intermediates in the plant defense response. *Proc Natl Acad Sci USA* 99:517–522.
29. Tissier AF, et al. (1999) Multiple independent defective suppressor-mutator transposon insertions in *Arabidopsis*: A tool for functional genomics. *Plant Cell* 11: 1841–1852.
30. Lee SC, et al. (2011) Molecular characterization of the submergence response of the *Arabidopsis thaliana* ecotype Columbia. *New Phytol* 190:457–471.
31. Chang KN, et al. (2013) Temporal transcriptional response to ethylene gas drives growth hormone cross-regulation in *Arabidopsis*. *eLife* 2:e00675.
32. Kim HJ, et al. (2014) Gene regulatory cascade of senescence-associated NAC transcription factors activated by ETHYLENE-INSENSITIVE2-mediated leaf senescence signalling in *Arabidopsis*. *J Exp Bot* 65:4023–4036.
33. Zhang K, Gan SS (2012) An abscisic acid-AtNAP transcription factor-SAG113 protein phosphatase 2C regulatory chain for controlling dehydration in senescing *Arabidopsis* leaves. *Plant Physiol* 158:961–969.
34. Zhang K, Xia X, Zhang Y, Gan SS (2012) An ABA-regulated and Golgi-localized protein phosphatase controls water loss during leaf senescence in *Arabidopsis*. *Plant J* 69: 667–678.
35. He XJ, et al. (2005) AtNAC2, a transcription factor downstream of ethylene and auxin signaling pathways, is involved in salt stress response and lateral root development. *Plant J* 44:903–916.
36. Balazadeh S, et al. (2010) A gene regulatory network controlled by the NAC transcription factor ANAC092/AtNAC2/ORE1 during salt-promoted senescence. *Plant J* 62: 250–264.
37. Qiu K, et al. (2015) EIN3 and ORE1 accelerate degreening during ethylene-mediated leaf senescence by directly activating chlorophyll catabolic genes in *Arabidopsis*. *PLoS Genet* 11:e1005399.
38. Buchanan-Wollaston V, et al. (2005) Comparative transcriptome analysis reveals significant differences in gene expression and signalling pathways between developmental and dark/starvation-induced senescence in *Arabidopsis*. *Plant J* 42: 567–585.
39. Ye Y, et al. (2017) A novel chemical inhibitor of ABA signaling targets all ABA receptors. *Plant Physiol* 173:2356–2369.
40. Elstner EF, Osswald W (1994) Mechanisms of oxygen activation during plant stress. *Proc R Soc Edinburgh Sect B Biol Sci* 102:131–154.
41. Smirnoff N (1995) Antioxidant systems and plant response to the environment. *Environment and Plant Metabolism: Flexibility and Acclimation*, ed Smirnoff N (BIOS Scientific, Oxford), pp 217–243.
42. Huang S, Van Aken O, Schwarzländer M, Belt K, Millar AH (2016) The roles of mitochondrial reactive oxygen species in cellular signaling and stress response in plants. *Plant Physiol* 171:1551–1559.
43. Baxter-Burrell A, Yang Z, Springer PS, Bailey-Serres J (2002) RopGAP4-dependent Rop GTPase rheostat control of *Arabidopsis* oxygen deprivation tolerance. *Science* 296: 2026–2028.
44. Pucciariello C, Parlanti S, Banti V, Novi G, Perata P (2012) Reactive oxygen species-driven transcription in *Arabidopsis* under oxygen deprivation. *Plant Physiol* 159: 184–196.
45. Mustroph A, et al. (2009) Profiling translatomes of discrete cell populations resolves altered cellular priorities during hypoxia in *Arabidopsis*. *Proc Natl Acad Sci USA* 106: 18843–18848.
46. Yao Y, et al. (2017) *ETHYLENE RESPONSE FACTOR 74* (*ERF74*) plays an essential role in controlling a respiratory burst oxidase homolog D (RbohD)-dependent mechanism in response to different stresses in *Arabidopsis*. *New Phytol* 213:1667–1681.
47. Akman M, Kleine R, van Tienderen PH, Schranz ME (2017) Identification of the submergence tolerance QTL *Come Quick Drowning1* (*CQD1*) in *Arabidopsis thaliana*. *J Hered* 108:308–317.
48. Setter TLT, et al. (2010) Desiccation of leaves after de-submergence is one cause for intolerance to complete submergence of the rice cultivar IR 42. *Funct Plant Biol* 37: 1096–1104.
49. Shahzad Z, et al. (2016) A potassium-dependent oxygen sensing pathway regulates plant root hydraulics. *Cell* 167:87–98.e14.
50. Tanaka Y, et al. (2005) Ethylene inhibits abscisic acid-induced stomatal closure in *Arabidopsis*. *Plant Physiol* 138:2337–2343.
51. Voesenek LACJ, et al. (2003) De-submergence-induced ethylene production in *Rumex palustris*: Regulation and ecophysiological significance. *Plant J* 33:341–352.
52. Porra RJ, Thompson WA, Kriedemann PE (1989) Determination of accurate extinction coefficients and simultaneous equations for assaying chlorophylls a and b extracted with four different solvents: Verification of the concentration of chlorophyll standards by atomic absorption spectroscopy. *Biochim Biophys Acta* 975:384–394.
53. Marsch-Martínez N, et al. (2013) An efficient flat-surface collar-free grafting method for *Arabidopsis thaliana* seedlings. *Plant Methods* 9:14.
54. Ingolia NT, Brar GA, Rouskin S, McGeachy AM, Weissman JS (2012) The ribosome profiling strategy for monitoring translation in vivo by deep sequencing of ribosome-protected mRNA fragments. *Nat Protoc* 7:1534–1550.
55. Juntawong P, Girke T, Bazin J, Bailey-Serres J (2014) Translational dynamics revealed by genome-wide profiling of ribosome footprints in *Arabidopsis*. *Proc Natl Acad Sci USA* 111:E203–E212.
56. Juntawong P, Hummel M, Bazin J, Bailey-Serres J (2015) Ribosome profiling: A tool for quantitative evaluation of dynamics in mRNA translation. *Plant Functional Genomics*, Methods in Molecular Biology, Vol 1284, eds Alonso J, Stepanova A (Humana, New York), pp 139–173.
57. Stewart RR, Bewley JD (1980) Lipid peroxidation associated with accelerated aging of soybean axes. *Plant Physiol* 65:245–248.
58. Zhang NX, et al. (2018) Phytophagy of omnivorous predator *Macrolophus pygmaeus* affects performance of herbivores through induced plant defences. *Oecologia* 186: 101–113.
59. Livak KJ, Schmittgen TD (2001) Analysis of relative gene expression data using real-time quantitative PCR and the 2(−Delta Delta C(T)) method. *Methods* 25:402–408.